J. Fluid Mech. (2014), *vol.* 758, *pp.* 553–564. © Cambridge University Press 2014
doi:10.1017/jfm.2014.545

Horizontal turbulent diffusion in a convective mixed layer

Junshi Ito[1,†], Hiroshi Niino[1] and Mikio Nakanishi[2]

[1]Atmosphere and Ocean Research Institute, The University of Tokyo, Kashiwa, Chiba, 277-8564, Japan

[2]National Defense Academy, Yokosuka, Kanagawa, 239-0811, Japan

(Received 3 June 2013; revised 5 July 2014; accepted 15 September 2014;
first published online 10 October 2014)

A large eddy simulation (LES) is used to estimate a reliable horizontal turbulent diffusion coefficient, K_h, in a convective mixed layer (CML). The introduction of a passive scalar field with a fixed horizontal gradient at a given time enables K_h estimation as a function of height, based on the simulated turbulent horizontal scalar flux. Here K_h is found to be of the order of 100 m^2 s^{-1} for a typical terrestrial atmospheric CML. It is shown to scale by the product of the CML convective velocity, w_*, and its depth, h. Here K_h is characterized by a vertical profile in the CML: it is large near both the bottom and top of the CML, where horizontal flows associated with convection are large. The equation pertaining to the temporal rate of change of a horizontal scalar flux suggests that K_h is determined by a balance between production and pressure correlation at a fully developed stage. Pressure correlation near the bottom of the CML is localized in convergence zones near the boundaries of convective cells and becomes large within an eddy turnover time, h/w_*, after the introduction of the passive scalar field.

Key words: buoyant boundary layers, mixing and dispersion, turbulent convection

1. Introduction

When a thermally stratified fluid is either heated from below or cooled from above, a convective mixed layer (CML) is formed, where release of potential energy results in vigorous turbulence. CMLs occur in a wide range of geophysical and astrophysical flows, such as in terrestrial and planetary atmospheres, oceans, the Earth's interior and stars. Like Rayleigh–Bénard convection, which results from both heating from the bottom and cooling from the top, CML dynamics have also been studied extensively (e.g. Plate *et al.* 1998).

Since individual convection cells in a CML are often characterized by much smaller horizontal scales than those of flows of interest, most numerical models pertaining to large-scale flows use horizontal grid sizes that do not resolve the convection cells. Thus, turbulent transport caused by convection must be parameterized. A number of studies have investigated parameterization of vertical turbulent transport in a CML for Reynolds-averaged Navier–Stokes (RANS) models (cf. Mironov 2009). Global to mesoscale numerical weather prediction models, which belong to a category of RANS

† Email address for correspondence: junshi@aori.u-tokyo.ac.jp

https://doi.org/10.1017/jfm.2014.545 Published online by Cambridge University Press

models, have employed some of these parameterizations (e.g. Mellor & Yamada 1974; Hong & Pan 1996; Nakanishi & Niino 2009). By contrast, physical processes that cause horizontal turbulent transport have attracted less interest. Such processes have not been studied in detail, partly because their effects are often masked by artificial diffusion aimed at suppressing numerical instabilities.

One of the important topics related to horizontal turbulent transport involves the dispersion of pollutants in the atmosphere. A number of attempts to parameterize horizontal turbulent diffusion for RANS models have been made (e.g. Chino & Ishikawa 1988; Byun & Schere 2006). Chino & Ishikawa (1988) used a Pasquill–Gifford chart (Gifford 1961) that semi-empirically determines a horizontal turbulent diffusion coefficient, K_h. Although K_h thus determined may be reliable for short downwind distances from a source, they may not be for long distances. Byun & Schere (2006) parameterized K_h based on the Smagorinsky model (Smagorinsky 1963) in a mesoscale atmospheric model to predict pollutant diffusion. However, the use of the Smagorinsky model in a mesoscale setting may not be rationalized when the grid size is outside the scale of an inertial subrange.

While the horizontal dispersion from a point source in CMLs has been studied extensively at short downwind distances of typically less than 1 km in which high concentration of pollutants can be generated (e.g. Gifford 1961; Weil *et al.* 2012), relatively little quantitative discussion based on field observation has been presented for horizontal dispersion in longer downwind distances that are larger than the horizontal scales of convection cells. This is partly because the dispersion in the real atmosphere is not only caused by convective motions, but also affected by time-varying environmental winds, mesoscale circulations such as sea breezes and local topographies. On the other hand, Willis & Deardorff (1981) performed a laboratory experiment on a CML to investigate horizontal dispersion for vertically integrated concentration of a passive scalar both in short and long distances.

Since RANS models which give accurate horizontal diffusion in a long downwind distance may be critically important on an occasion such as the accidental emission of radioactive material from a nuclear power plants in Fukushima, Japan (e.g. Morino, Ohara & Nishizawa 2011), a reliable formulation of K_h is desired. However, our understanding of horizontal diffusion is not sufficient even for an idealized CML: we need to know basic characteristics of horizontal diffusion in a CML such as its scaling and vertical profile of K_h.

On the basis of a large eddy simulation (LES) with a sufficiently high resolution to resolve turbulent eddies in a CML, the present study examines basic processes of horizontal turbulent transport. Hotta, Iida & Yokoyama (2012) studied numerically the horizontal dispersion of a passive scalar in the presence of Rayleigh–Bénard convection. The initial distribution of the passive scalar was given by a Gaussian function, and an estimate of K_h only for vertically integrated concentration was desired. In the present paper, we introduce a novel way to reliably estimate K_h: at a certain time after the CML is developed, a passive scalar field having a fixed uniform horizontal gradient is introduced, and the resulting horizontal turbulent flux is used to obtain the vertical profile of K_h, which may in turn be used for improving a parameterization of horizontal turbulent transport in a RANS model.

The remainder of this paper is organized as follows. In § 2 the experimental setting is described. The horizontal diffusion coefficient is estimated in § 3, and the simulation results are discussed in § 4. Finally, concluding remarks are presented in § 5.

https://doi.org/10.1017/jfm.2014.545 Published online by Cambridge University Press

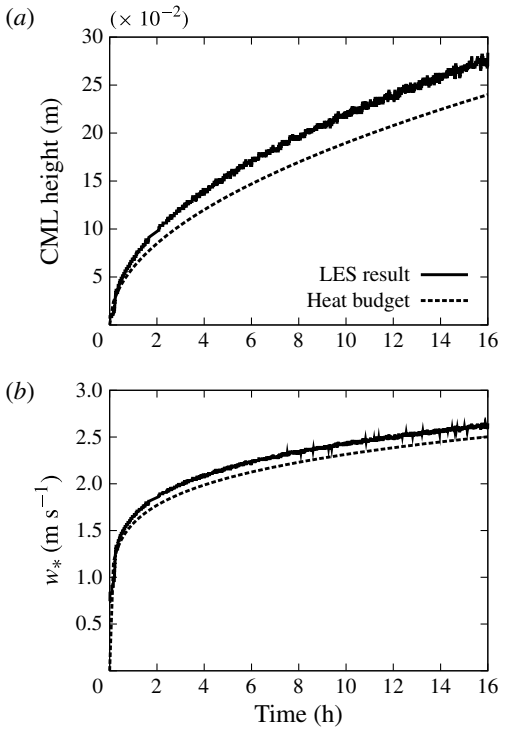


FIGURE 1. Time series of (*a*) CML h and (*b*) convective velocity, $w_* \equiv (gQh/\theta)^{\frac{1}{3}}$ (solid lines) for $Q = 0.2$ K m s^{-1}. The dashed lines show the predictions associated with a heat budget.

2. Numerical setting

The three-dimensional LES model employed in the present study was developed by Ito, Niino & Nakanishi (2010*a*,*b*). It employs the Boussinesq approximation and Smagorinsky's subgrid-scale (SGS) model (for details, see the Appendix of Ito *et al.* 2010*a*) on the Arakawa C-grid. CMLs reproduced by our LES code are similar to those simulated by different codes in the presence of weak environmental shear (Fedorovich *et al.* 2004).

A uniform grid size of 25 m in all three dimensions is used. The horizontal size of the calculation domain is 18 km × 18 km, and the vertical extent is 5 km. The top boundary is free-slip and adiabatic, whereas the lateral boundaries are cyclic. No ambient wind is included. The initial potential temperature increases linearly with height at a constant rate, Γ, of 4.0 K km^{-1} from its surface value of 299 K. A constant kinematic heat flux, $Q = 0.2$ or 0.1 K m s^{-1}, is adopted at the surface to develop a CML. The surface stress is calculated using the bulk method, which is based on the Monin–Obukhov similarity law. Time integration is performed with a time step of 0.2 s. As examined in Appendix, the grid size and time step are fine enough for the purpose of this study.

The CML continually grows because of the positive heat flux at the surface. Figure 1 shows time series of the CML depth, h and the convective velocity scale, $w_* \equiv (ghQ/\theta_0)^{1/3}$ (Deardorff 1970), for $Q = 0.2$ K m s^{-1}, where $g = 9.81$ m s^{-2} represents the acceleration due to gravity and $\theta_0 = 309$ K is the standard potential

https://doi.org/10.1017/jfm.2014.545 Published online by Cambridge University Press

temperature. The depth h is defined as the height where the horizontally averaged vertical heat flux takes the minimum value. The development of h agrees reasonably well with predictions based on a heat budget of $0.5 \times \Gamma h^2 = Qt$ (see figure 1) at time t. Note that a slight systematic difference occurs at the top of the CML due to entrainment.

To investigate the horizontal turbulent diffusivity in the CML, a passive scalar field, C, characterized by a uniform horizontal gradient in the y direction, $\partial C/\partial y = -1$, is introduced at a given time. If the concentration of the passive scalar field, c, is denoted by $c = C + \hat{c} + c'$, where $\hat{c}$ and c' are the resolved and SGS deviations, respectively, from the basic field characterized by the uniform gradient, a prognostic equation for $\hat{c}$ is given by

$$\frac{\partial \hat{c}}{\partial t} = -\hat{u}\frac{\partial \hat{c}}{\partial x} - \hat{v}\frac{\partial C}{\partial y} - \hat{v}\frac{\partial \hat{c}}{\partial y} - \hat{w}\frac{\partial \hat{c}}{\partial z} + \frac{\partial}{\partial x}\left(\nu_\theta \frac{\partial \hat{c}}{\partial x}\right) + \frac{\partial}{\partial y}\left(\nu_\theta \frac{\partial C}{\partial y}\right) + \frac{\partial}{\partial y}\left(\nu_\theta \frac{\partial \hat{c}}{\partial y}\right) + \frac{\partial}{\partial z}\left(\nu_\theta \frac{\partial \hat{c}}{\partial z}\right), \tag{2.1}$$

where $\hat{u}$, $\hat{v}$ and $\hat{w}$ are the resolved velocity components in the x, y and z directions, respectively, and ν_θ represents the eddy diffusivity based on the zero-equation Smagorinsky's SGS model, which determines ν_θ diagnostically (Ito *et al.* 2010*a*). Note that $\hat{c}$ is assumed to be periodic horizontally. Equation (2.1) is integrated together with prognostic equations for $\hat{u}$, $\hat{v}$, $\hat{w}$ and the potential temperature.

3. Horizontal eddy diffusivity

Horizontal eddy diffusivity, K_h, is defined as

$$K_h \equiv -\langle vc\rangle \Big/ \frac{\partial C}{\partial y} = \langle \hat{v}\hat{c}\rangle + \langle v'c'\rangle = \langle \hat{v}\hat{c}\rangle - \left\langle \nu_\theta \frac{\partial \hat{c}}{\partial y}\right\rangle - \left\langle \nu_\theta \frac{\partial C}{\partial y}\right\rangle = \langle \hat{v}\hat{c}\rangle - \left\langle \nu_\theta \frac{\partial \hat{c}}{\partial y}\right\rangle + \langle \nu_\theta\rangle, \tag{3.1}$$

where the brackets denote Reynolds averages, which are estimated here as horizontal averages over the entire domain. Note that taking Reynolds averages eliminates products of resolved and SGS variables such as $\langle \hat{v}c'\rangle$ and $\langle v'\hat{c}\rangle$ in the third expression, in the final expression, the second and third terms represent SGS fluxes, which are always by two orders of magnitude less than the first term.

For experiments where $\partial C/\partial y$ is introduced at $t = 5$ h and $Q = 0.2$ K m s^{-1}, time series of K_h at different heights are shown in figure 2. At the instant when $\partial C/\partial y$ is introduced, $K_h = 0$, since $\hat{c} = 0$. Here K_h increases rapidly and fully develops after approximately 30 min, which is close to the convection's turnover time, h/w_*.

Here K_h then increases gradually as the CML grows. In the present CML, typical values of K_h are of the order of 100 m^2 s^{-1}, whereas K_h is much smaller above the CML (at $z = 1.25h$), where turbulent motions occur only sporadically. In addition to these fluctuations, K_h seems to have maxima near the top and bottom of the CML, where the horizontal convective velocities are large, as suggested by Dosio *et al.* (2005).

To show the evolution of the vertical profile clearly, figure 3(*a*) shows time averages of K_h for a duration of 1.5 h at different heights during its fully developed stage, which is attained 30 min after the introduction of $\partial C/\partial y$. Results of experiments in which $Q = 0.2$ K m s^{-1} and $\partial C/\partial y$ is introduced at $t = 5$, 7, 12 and 18 h after the start of the LES are shown. Also shown are the results of an experiment in which

https://doi.org/10.1017/jfm.2014.545 Published online by Cambridge University Press

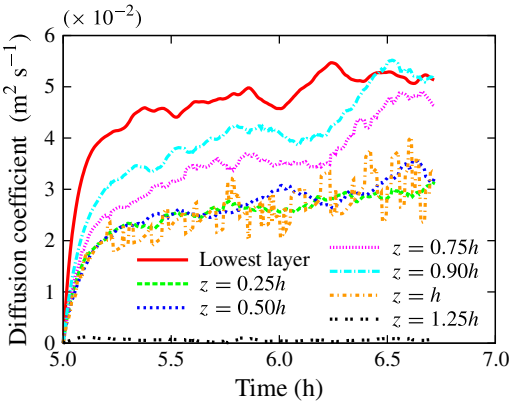


FIGURE 2. Temporal variations of K_h, estimated based on (3.1) at various heights. The passive scalar field horizontal gradient is imposed at $t = 5$ h from the start of the calculation.

$Q = 0.1$ K m s^{-1} and $\partial C/\partial y$ is introduced at $t = 8$ h after the start of the LES. For a fixed surface heat flux of $Q = 0.2$ K m s^{-1}, K_h increases with time as the CML develops.

Figure 3(*b*) is similar to figure 3(*a*), except that K_h is scaled by $w_* h$. The fully developed values of the non-dimensional coefficient K_h for different surface heat fluxes and different times nearly approach a single vertical profile. Whereas the dimensional K_h as shown in figure 3(*a*) is specific to the present setting (for which a terrestrial atmosphere has been assumed), the non-dimensional $K_h/w_* h$ as shown in figure 3(*b*) is applicable to a variety of CMLs that prevail in nature and engineering.

4. Discussion

In the present experiment, $\partial C/\partial y$ is fixed, so that K_h is solely determined by the horizontal flux, $\langle vc \rangle \sim \langle \hat{v}\hat{c} \rangle$. The equation for the temporal rate of change of $\langle \hat{v}\hat{c} \rangle$ is given by

$$\frac{\partial}{\partial t}\langle \hat{v}\hat{c} \rangle = -\langle \hat{v}^2 \rangle \frac{\partial C}{\partial y} - \frac{\partial}{\partial z}\langle \hat{v}\hat{w}\hat{c} \rangle + \left\langle \hat{p}\frac{\partial \hat{c}}{\partial y} \right\rangle + \epsilon, \tag{4.1}$$

where the first term on the right-hand side represents the production, the second term turbulent transport, the third term pressure correlation with $\hat{p}$ denoting the resolved-scale kinematic pressure and the fourth term the SGS contribution, which turns out to play a minor role. Note that horizontal turbulent transport $\partial\langle \hat{v}\hat{u}\hat{c} \rangle/\partial x$ and $\partial\langle \hat{v}^2\hat{c} \rangle/\partial y$ are dropped off because of the periodicities for horizontal directions. At the fully developed stage, the terms on the right-hand side should almost balance each other.

Figure 4(*a*,*b*) show vertical profiles of the terms in (4.1) at a developing stage of $\langle \hat{v}\hat{c} \rangle$ and at its fully developed stage, respectively, after introduction of the uniform horizontal gradient of the scalar field c where the terms are scaled by w_*^2. Note that the production term is solely determined by $\langle \hat{v}^2 \rangle$. The vertical profile of $\langle \hat{v}^2 \rangle/(w_*)^2$, shown by the solid line in figure 4, agrees well with the profile found in previous observational and numerical CML studies (e.g. Schmidt & Schumann 1989).

The magnitude of K_h is almost entirely determined by the balance between production and pressure correlation, except near the bottom of the CML. While the

https://doi.org/10.1017/jfm.2014.545 Published online by Cambridge University Press

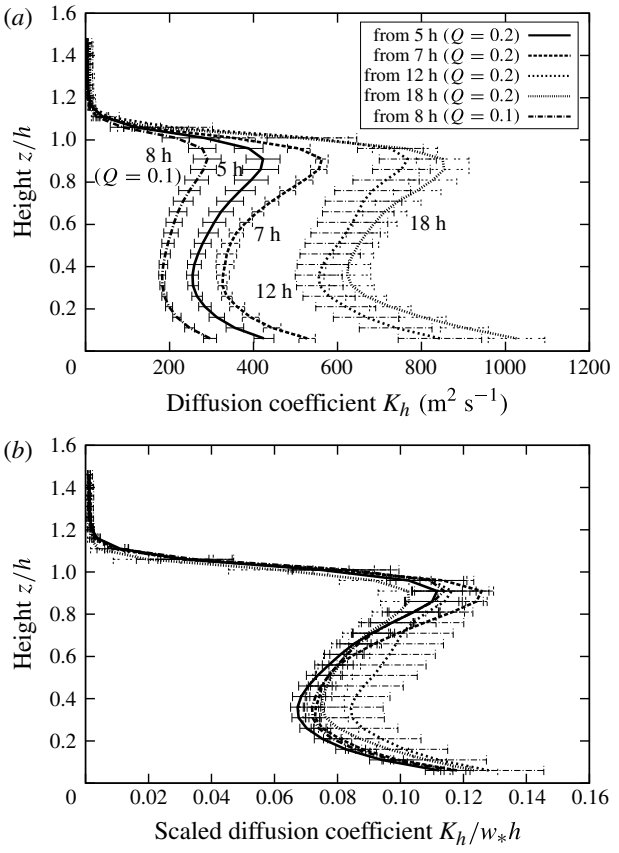


FIGURE 3. Vertical profiles of fully developed, time-averaged (*a*) K_h and (*b*) scaled K_h/w_*h. Full development of K_h is attained 30 min after $\partial C/\partial y$ is introduced. The standard deviations are shown as horizontal error bars. The averages and standard deviations are based on K_h measurements obtained every minute for a total duration of 1.5 h.

pressure correlation is almost uniform, the production exhibits peaks near both the ground and the top of the CML, where vertical turbulent transport of $\langle \hat{v}\hat{c} \rangle$ works to compensate for the imbalance.

Figure 5 shows the distribution of $\hat{c}$ and of the flow fields at a low level ($z \sim 0.06h$) of the CML at its fully developed stage ($t = 8$ h) corresponding to figure 4(*b*). Flows in the positive (negative) y direction tend to be associated with positive (negative) $\hat{c}$ because of the $\partial C/\partial y = -1$ gradient. Figure 6(*a*) shows the horizontal distribution of the pressure correlation term at low levels. Note that an additional horizontal filter averaging over grid points within a square with a side of 150 m, has been applied to the pressure correlation term to remove small-scale fluctuations. Convergence from opposite y directions results in positive deviations of $\hat{p}$ and a negative $\partial \hat{c}/\partial y$ gradient, so that the pressure correlation tends locally to lead to large negative values at the cell boundaries that are characterized by updrafts (see figure 6*a*). A similar process occurs near the top of the CML, and large negative values of pressure correlation are associated with downdraft regions at the centres of cells. By contrast, production has relatively uniform values across the domain (see figure 6*b*). These results show that

https://doi.org/10.1017/jfm.2014.545 Published online by Cambridge University Press

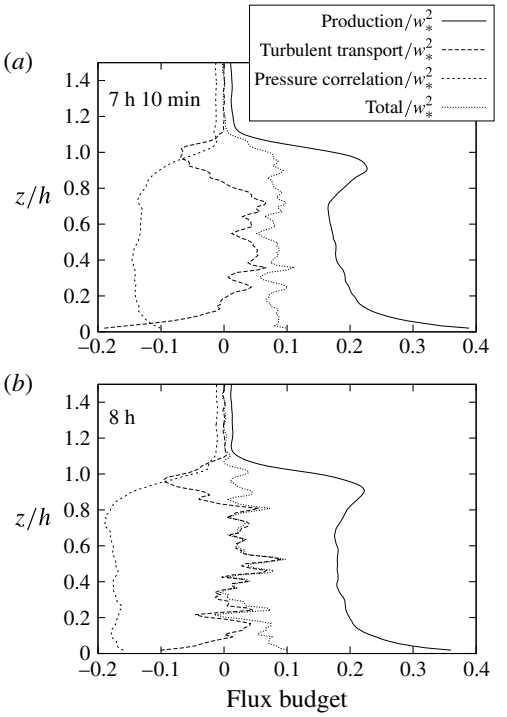


FIGURE 4. Vertical profiles of the terms on the right-hand side of (4.1) at (*a*) $t =$ 7 h 10 min and (*b*) $t = 8$ h, where the horizontal gradient of the passive scalar field is introduced at $t = 7$ h after the start of the calculation. Note that the height is scaled by h and that all terms are scaled by w_*^2.

pressure correlation and production are not balanced locally, although they are nearly balanced when averaged over the horizontal domain containing several convection cells. Thus, the K_h values obtained in the present study are only applicable to scalar-field gradients on horizontal scales larger than the convection cells.

Comparing figure 4(*a*,*b*), we note that the pressure correlation at $t = 7$ h 10 min is not as large as that at $t = 8$ h, and that it is not balanced with the production term. The smaller pressure correlation causes a rapid increase of K_h soon after the introduction of the uniform gradient at $t = 7$ h. This initial behaviour of K_h can be explained easily if the temporal rate of change of $\langle \hat{v}\hat{c} \rangle$ is rewritten in terms of an autocorrelation function, $R(\tau) \equiv \langle \hat{v}(t)\hat{v}(t+\tau) \rangle / \langle \hat{v}^2(t) \rangle$:

$$\begin{aligned} \frac{\partial}{\partial t}\langle \hat{v}\hat{c} \rangle &= \left\langle \frac{\partial}{\partial t}(\hat{v}\hat{c}) \right\rangle = \left\langle \frac{\mathrm{d}}{\mathrm{d}t}(\hat{v}\hat{c}) \right\rangle - \left\langle \frac{\partial(\hat{v}\hat{w}\hat{c})}{\partial z} \right\rangle \\ &\sim \left\langle \frac{\mathrm{d}}{\mathrm{d}t}(\hat{v}\hat{c}) \right\rangle = \left\langle \frac{\mathrm{d}}{\mathrm{d}t}\left(\hat{v} \int_0^t \hat{v}\,\mathrm{d}t \right) \right\rangle \\ &\sim \frac{\mathrm{d}}{\mathrm{d}t}\left(\langle \hat{v}(0)^2 \rangle \int_0^t R(\tau)\,\mathrm{d}\tau \right), \end{aligned} \tag{4.2}$$

where $\mathrm{d}/\mathrm{d}t$ denotes the Lagrangian (temporal) rate of change. Note that, to derive the second equality, the continuity equation and lateral periodicities are used and SGS

https://doi.org/10.1017/jfm.2014.545 Published online by Cambridge University Press

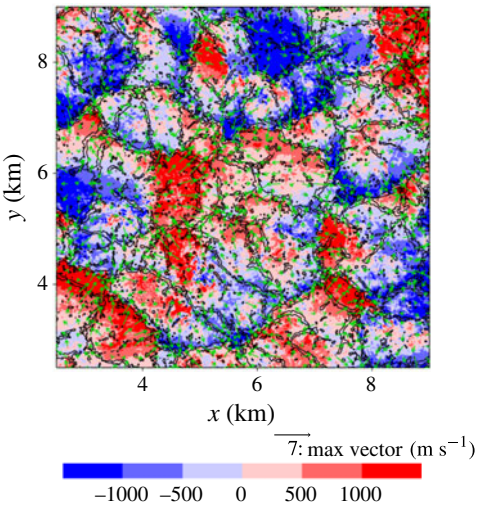


FIGURE 5. The distribution of $\hat{c}$ (colour shading) and horizontal wind vectors (green arrows) in a horizontal section at $z = 112.5$ m ($\sim 0.06h$) at $t = 8$ h after the start of the LES. Note that only a section of the calculation domain is shown. Updraft regions where $\hat{w} > 1$ m s^{-1} are shown by black isolines.

contributions are neglected; we have also used $\mathrm{d}\hat{c}/\mathrm{d}t \sim -\hat{v}\partial C/\partial y = \hat{v}$ from (2.1) and neglected SGS contributions and vertical turbulent advection (cf. figure 4) to derive the third equality; steadiness of $\langle v(t)\rangle$ and $R(\tau)$ is assumed in the final equality. Equation (4.2) shows that the behaviour of $K_h \sim \langle \hat{v}\hat{c}\rangle$ is explained in a similar way to the derivation of Taylor's diffusion theory (cf. Panofsky & Dutton 1983, p. 238). Since $R(t) \to 1$ for $t \to 0$, $\langle \hat{v}\hat{c}\rangle = K_h$ initially increases linearly with time. On the other hand, K_h tends to a constant because $R(t) \to 0$ after the eddy turnover time, h/w_*, when particles move from their initial positions to reach convergence zones of convective cells.

Using a laboratory experiment in which a continuous point source is placed in a CML with a weak environmental wind, Willis & Deardorff (1981) suggested that crosswind dispersion, σ_y, for vertically integrated concentration in a downwind distance satisfying $xU/w_*h > 2$ is given by $\sigma_y/h = 0.36 \times (w_* t/h)^{1/2}$, where x is downwind distance from the point source, U environmental wind speed and t elapsed time after the passive scalar is released from the source. If the relationship $\sigma_y \sim \sqrt{2K_h t}$ between the crosswind dispersion σ_y and horizontal diffusivity K_h as obtained from a solution of the one-dimensional diffusion equation (Panofsky & Dutton 1983, p. 231) is considered, their result corresponds to $K_h/w_*h \sim (0.36)^2/2 \sim 0.065$, which is somewhat small compared with ours (figure 3*b*). The difference may possibly be caused by the passive scalar in their experiment not being vertically well mixed even for $xU/w_*h > 2$. Based on a LES, Weil *et al.* (2012) also made a similar study to Willis & Deardorff (1981). Their figure 9 suggests that crosswind dispersion, σ_y/h, for $t = h/w_*$ is 0.3–0.4 depending on the source height, which gives $K_h/w_*h \sim 0.045$–0.08 if (4.3) is used. These values are again somewhat smaller than ours.

Weil *et al.* (2012) also plotted crosswind dispersion data obtained by the field experiment CONDORS (COnvective Diffusion Observed by Remote Sensors; Eberhard, Moninger & Briggs 1988; Briggs 1993) in their figure 9. The crosswind dispersion, σ_y/h, for $t = h/w_*$ in the field experiment is generally larger than that

https://doi.org/10.1017/jfm.2014.545 Published online by Cambridge University Press

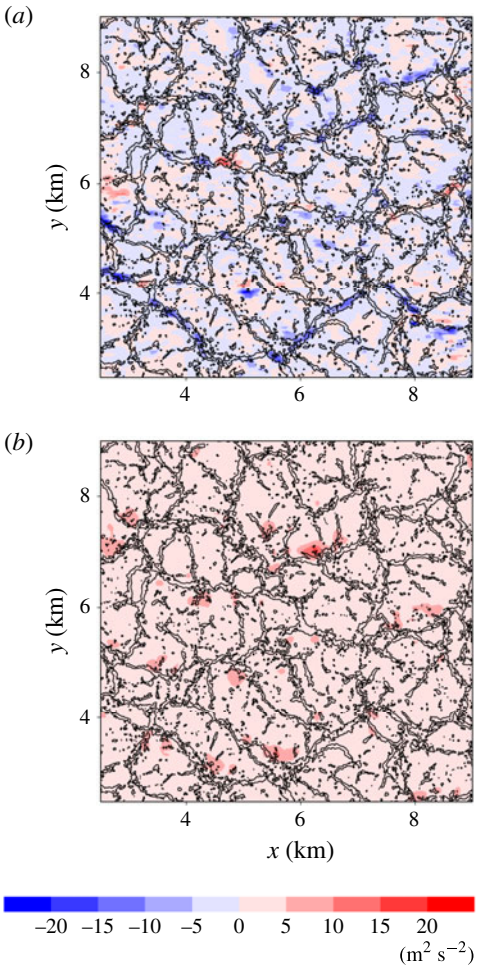


FIGURE 6. As for figure 5, except (*a*) for filtered pressure correlation $\overline{\hat{p}(\partial\hat{c}/\partial y)}$ and (*b*) for the production term, where the overbar denotes a filtered quantity which is obtained by averaging over grid points within a 150 m square to remove small-scale fluctuations.

obtained by the LES, and that obtained for an elevated point source is 0.4–0.9, which gives $K/w_* h \sim 0.08$–0.41. The larger values of the horizontal diffusivity in the field experiments are likely to be caused by local circulations due to thermal contrast and topographies. Several previous observations in the real atmosphere also suggested larger values for K_h for longer diffusion times (∼several days) (Gifford 1982). Gifford (1982) and Panofsky & Dutton (1983, p. 231) suggest that the larger values of K_h are likely to result from local circulations (such as sea-breeze circulations) which have larger horizontal scales than the convection cells. Such local circulations are not present in our study, since we have assumed statistical homogeneity in the horizontal direction. In fact, Terada, Nagai & Yamazawa (2013) suggests that eddy diffusivity of Gifford (1982) should be reduced if resolution of numerical model is improved to resolve such local circulations.

We briefly discuss a comparison with the conventional parameterization given by the Pasquill–Gifford chart that gives a relationship between crosswind dispersion σ_y and

https://doi.org/10.1017/jfm.2014.545 Published online by Cambridge University Press

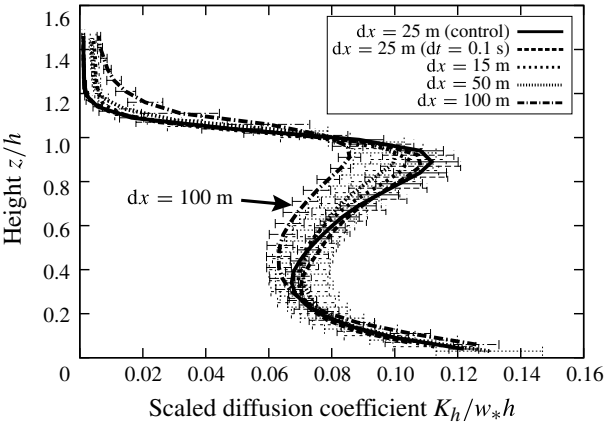


FIGURE 7. Vertical profiles of fully developed, time-averaged scaled K_h/w_*h for sensitivity experiments presented in the same way as figure 3(*b*), where $Q = 0.2$ K m s^{-1} and the passive scalar field's horizontal gradient is imposed at $t = 5$ h.

downwind distance x. The corresponding horizontal diffusion coefficient $K_p = \sigma_y^2 U/2x$ monotonically increases with a certain power of x, where σ_y increases nearly with $x^{0.9}$. When $x = 6$ km, the chart indicates $\sigma_y \sim 1$ km in the unstable case. If a typical value of $U = 2$ m s^{-1} is assumed, K_p results in 170 m^2 s^{-1}, which is slightly larger than the value of K_H obtained in the present study. Note that when the environmental wind vanishes as in the present LES, however, the formulation of K_p does not remain valid.

5. Concluding remarks

Horizontal diffusion due to turbulent motions in a CML is investigated by means of a LES in which a uniform horizontal gradient of a passive scalar is introduced at a certain instant. The LES shows that the horizontal diffusion coefficient, K_h, is of the order of 100 m^2 s^{-1} for a typical terrestrial atmospheric CML. It is found that K_h scales with the product of w_* and h, where w_* is the convective velocity scale and h the CML depth. Here K_h has a universal vertical profile (see, e.g., figure 3*b*), which needs to be considered when parameterizing the horizontal diffusion in a CML. Note that a CML horizontal turbulent diffusivity is not proportional to the vertical turbulent diffusion coefficient, which has a maximum in the middle of the CML (see figure 2 in Degrazia *et al.* (1997) that presents a vertical profile of non-dimensional vertical turbulent diffusion coefficient). The results of this study can be applied not only to CMLs in the terrestrial atmosphere but also to those in the atmospheres of other planets and stars, the lakes and the oceans.

Acknowledgements

This work was supported by Field 3, Strategic Programs for Innovative Research, the Japanese Government's MEXT, and JSPS KAKENHI grant number 23221001. We would like to thank three anonymous reviewers for helpful suggestions and comments. The computation was carried out using the computer facilities at both the Atmosphere and Ocean Research Institute, the University of Tokyo and the Meteorological Research Institute of JMA.

https://doi.org/10.1017/jfm.2014.545 Published online by Cambridge University Press

Appendix. Sensitivities on grid size and time step

In this appendix, we will examine sensitivities of horizontal turbulent diffusivity on grid size and time step. First, the same experiment as the control, which utilized a grid size dx of 25 m, was made with d$x = 100$, 50, and 15 m, while keeping the domain size and time step. Figure 7 shows that the scaled diffusion coefficient nearly converges if dx is less than or equal to 25 m.

Also plotted in figure 7 is the scaled diffusion coefficient for the same experiment as the control except that the time step is reduced by half. The difference between the two experiments is small, demonstrating that the results depend little on time step if it is less than or equal to 0.2 s.

REFERENCES

BRIGGS, G. A. 1993 Plume dispersion in the convective boundary layer. Part II: analyses of CONDORS field experiment data. *J. Appl. Meteorol.* **32**, 1388–1425.

BYUN, D. & SCHERE, K. L. 2006 Review of the governing equations, computational algorithms, and other components of the models: 3. Community Multiscale Air Quality (CMAQ) modeling system. *Appl. Mech. Rev.* **59**, 51–77.

CHINO, M. & ISHIKAWA, H. 1988 Experimental verification study for system for prediction of environmental emergency dose information: SPEEDI, (ii). *J. Nucl. Sci. Technol.* **25**, 805–815.

DEARDORFF, J. W. 1970 Convective velocity and temperature scales for the unstable planetary boundary layer and for Rayleigh convection. *J. Atmos. Sci.* **27**, 1211–1213.

DEGRAZIA, G. A., RIZZA, U., MANGIA, C. & TIRABASSI, T. 1997 Validation of a new turbulent parameterization for dispersion models in convective conditions. *Boundary-Layer Meteorol.* **85**, 243–254.

DOSIO, A., GUERAU DE ARELLANO, J. V., HOLTSLAG, A. A. M. & BUILTJES, P. J. H. 2005 Relating Eulerian and Lagrangian statistics for the turbulent dispersion in the atmospheric convective boundary layer. *J. Atmos. Sci.* **62**, 1175–1191.

EBERHARD, W. L., MONINGER, W. R. & BRIGGS, G. A. 1988 Plume dispersion in the convective boundary layer. Part I: CONDORS field experiment and example measurements. *J. Appl. Meteorol.* **27**, 599–616.

FEDOROVICH, E., CONZEMIUS, R., ESAU, I., CHOW, F. K., LEWELLEN, D., MOENG, C.-H., SULLIVAN, P., PINO, D. & DE ARELLANO, J.-G. 2004 Entrainment into sheared convective boundary layers as predicted by different large eddy simulation codes. In *16th Symposium on Boundary Layers and Turbulence*.

GIFFORD, F. A. 1961 Use of routine meteorological observations for estimating atmospheric dispersion. *Nucl. Safety* **2**, 47–51.

GIFFORD, F. A. 1982 Horizontal diffusion in the atmosphere: a Lagrangian-dynamical theory. *Atmos. Environ.* **16**, 505–512.

HONG, S. Y. & PAN, H. L. 1996 Nonlocal boundary layer vertical diffusion in a medium-range forecast model. *Mon. Weath. Rev.* **124**, 2322–2339.

HOTTA, H., IIDA, Y. & YOKOYAMA, T. 2012 Estimation of turbulent diffusivity with direct numerical simulation of stellar convection. *Astrophys. J. Lett.* **751**, L9.

ITO, J., NIINO, H. & NAKANISHI, M. 2010*a* Large eddy simulation of dust devils in a diurnally-evolving convective mixed layer. *J. Met. Soc. Japan* **88**, 64–77.

ITO, J., NIINO, H. & NAKANISHI, M. 2010*b* Large eddy simulation on dust suspension in a convective mixed layer. *SOLA* **6**, 133–136.

MELLOR, G. L. & YAMADA, T. 1974 A hierarchy of turbulence closure models for planetary boundary layers. *J. Atmos. Sci.* **31**, 1791–1806.

MIRONOV, D. V. 2009 Turbulence in the lower troposphere: second-order closure and mass-flux modelling frameworks. In *Interdisciplinary Aspects of Turbulence*, Lecture Notes in Physics, vol. 756, pp. 1–61. Springer.

https://doi.org/10.1017/jfm.2014.545 Published online by Cambridge University Press

MORINO, Y., OHARA, T. & NISHIZAWA, M. 2011 Atmospheric behavior, deposition, and budget of radioactive materials from the Fukushima Daiichi nuclear power plant in March 2011. *Geophys. Res. Lett.* **38**, L00G11.

NAKANISHI, M. & NIINO, H. 2009 Development of an improved turbulence closure model for the atmospheric boundary layer. *J. Met. Soc. Japan* **87**, 895–912.

PANOFSKY, H. A. & DUTTON, J. A. 1983 *Atmospheric Turbulence*. Wiley-Interscience.

PLATE, E. J., FEDOROVICH, E. E., VIEGAS, D. X. & WYNGAARD, J. C. 1998 *Buoyant Convection in Geophysical Flows*. Kluwer Academic.

SCHMIDT, H. & SCHUMANN, U. 1989 Coherent structure of the convective boundary layer derived from large-eddy simulations. *J. Fluid Mech.* **200**, 511–562.

SMAGORINSKY, J. 1963 General circulation experiments with the primitive equations. 1. The basic experiment. *Mon. Weather Rev.* **91**, 99–164.

TERADA, H., NAGAI, H. & YAMAZAWA, H. 2013 Validation of a Lagrangian atmospheric dispersion model against middle-range scale measurements of 85Kr concentration in Japan. *J. Nucl. Sci. Technol.* **50**, 1198–1212.

WEIL, J. C., SULLIVAN, P., PATTON, E. & MOENG, C.-H. 2012 Statistical variability of dispersion in the convective boundary layer: ensembles of simulations and observations. *Boundary-Layer Meteorol.* **145**, 185–210.

WILLIS, G. E. & DEARDORFF, J. W. 1981 A laboratory study of dispersion from a source in the middle of the convectively mixed layer. *Atmos. Environ.* **15**, 109–117.

https://doi.org/10.1017/jfm.2014.545 Published online by Cambridge University Press